How to cite: *Angew. Chem. Int. Ed.* **2024**, *63*, e202401372
doi.org/10.1002/anie.202401372

Single-Molecule Magnets

Unique Double and Triple Decker Arrangements of Rare-Earth 9,10-Diborataanthracene Complexes Featuring Single-Molecule Magnet Characteristics

Cedric Uhlmann, Luca Münzfeld, Adrian Hauser, Ting-Ting Ruan, Senthil Kumar Kuppusamy, Chengyu Jin, Mario Ruben, Karin Fink, Eufemio Moreno-Pineda, and Peter W. Roesky**

Dedicated to Prof. Rhett Kempe on the occasion of his 60th birthday

Abstract: Herein, we present the first report on the synthesis of rare-earth complexes featuring a 9,10-diborataanthracene ligand. This 14-π-electron ligand is highly reductive and was previously used in small-molecule activation. Salt elimination reactions between dipotassium 9,10-diethyl-9,10-diborataanthracene [K_2(DEDBA)] and [$Ln^{III}(\eta^8\text{-}Cot^{TIPS})(BH_4)(thf)_x$] ($Cot^{TIPS}$ = 1,4-($^iPr_3Si)_2C_8H_6$) in a 1:1 ratio yielded heteroleptic sandwich complexes [$K(\eta^8\text{-}Cot^{TIPS})Ln^{III}(\eta^6\text{-}DEDBA)$] (Ln = Y, Dy, Er). These compounds form Lewis-base-free one-dimensional coordination polymers when crystallised from toluene. In contrast, reaction of [K_2(DEDBA)] and [$Ln^{III}(\eta^8\text{-}Cot^{TIPS})(BH_4)(thf)_x$] in a 1:2 ratio led to the formation of heteroleptic triple-decker complexes [$(\eta^8\text{-}Cot^{TIPS})Ln^{III}(\mu\text{-}\eta^6\text{:}\eta^6\text{-}DEDBA)Ln^{III}(\eta^8\text{-}Cot^{TIPS})$] (Ln = Y, Dy, Er). Notably, these are not only the first lanthanide triple-decker compounds featuring a six-membered ring as a deck but also the first trivalent lanthanide triple-decker featuring a heterocycle in the coordination sphere. Magnetic investigations reveal that [$K(\eta^8\text{-}Cot^{TIPS})Ln^{III}(\eta^6\text{-}DEDBA)$] (Ln = Dy, Er) and [$(\eta^8\text{-}Cot^{TIPS})Er^{III}(\mu\text{-}\eta^6\text{:}\eta^6\text{-}DEDBA)Er^{III}(\eta^8\text{-}Cot^{TIPS})$] exhibit Single-Molecule Magnet (SMM) behaviour. In the case of [$(\eta^8\text{-}Cot^{TIPS})Ln^{III}(\mu\text{-}\eta^6\text{:}\eta^6\text{-}DEDBA)Ln^{III}(\eta^8\text{-}Cot^{TIPS})$] (Ln = Dy, Er), the introduction of a second near lanthanide ion results in strong antiferromagnetic interactions, allowing the enhancement of the magnetic characteristic of the system, compared to the quasi isolated counterpart. This research renews the overlooked coordination chemistry of the DBA ligand and expands it to encompass rare-earth elements.

Introduction

The discovery of ferrocene [$(\eta^5\text{-}Cp)_2Fe$] (Cp = C_5H_5) by Kealy and Pauson marked the beginning of modern-day organometallic chemistry and defined the class of metallocenes or sandwich complexes.[1] In a sandwich complex, the central metal is exclusively coordinated by two cyclic and planar ligands via π-bonds. Ever since there has been an ongoing search for novel metallocenes comprising a variety of metals and π-cyclic ligands. Metallocenes, in particular lanthanocenes, play an important role, especially in catalysis, small-molecule activation, and scaffolding for data storage devices or Quantum Information Processing (QIP).[2] Besides pure carbon-based ligands, a great number of hetero-

[*] C. Uhlmann, L. Münzfeld, A. Hauser, P. W. Roesky
Institute of Inorganic Chemistry, Karlsruhe Institute of Technology (KIT), Engesserstraße 15, 76131 Karlsruhe
E-mail: roesky@kit.edu

T.-T. Ruan, C. Jin, M. Ruben, K. Fink
Institute of Nanotechnology, Karlsruhe Institute of Technology (KIT), Kaiserstraße 12, 76131 Karlsruhe, Germany

S. Kumar Kuppusamy, M. Ruben
Institute of Quantum Materials and Technologies (IQMT), Karlsruhe Institute of Technology (KIT), 76344 Eggenstein-Leopoldshafen, Germany

M. Ruben
Centre Européen de Science Quantique (CESQ); Institut de Science et d'Ingénierie Supramoléculaires (ISIS, UMR 7006), CNRS-Université de Strasbourg, 8 allée Gaspard Monge BP 70028 67083 Strasbourg Cedex, France

E. Moreno-Pineda
Universidad de Panamá, Facultad de Ciencias Naturales, Exactas y Tecnología, Depto. de Química-Física, Panamá, 0824, Panamá
E-mail: eufemio.moreno@up.ac.pa

E. Moreno-Pineda
Universidad de Panamá, Facultad de Ciencias Naturales, Exactas y Tecnología, Grupo de Investigación de Materiales, Panamá, 0824, Panamá

cycles have also been employed for the construction of sandwich complexes. For instance, pioneering work in the 1980s by Siebert et al. and Herberich et al. unveiled early examples of triple-decker complexes using boraheterocycles as ligands.[3] In general, the 6π aromatic nature of the parent cyclopentadienide monoanion and benzene is retained by the replacement of a CH by a BH^- fragment, due to the isolobal analogy. The corresponding aromatic dianionic borole and monoanionic boratabenzene are available for the construction of sandwich complexes.[4] Although these ligands have been well-known in d-block chemistry for decades, the number of sandwich complexes with boraheterocylces is limited.[5] Three prominent examples of sandwich complexes bearing boron heterocycles coordinated to lanthanides are: (*i*) a complex $[Er^{III}(\eta^6\text{-}C_5H_5BMe)(\eta^8\text{-}Cot)]$ in which a monoanionic boratabenzene and a cycloocatetraendiide co-ligand has been used (Figure 1A);[5c] (*ii*) the work from Nippe et al. whom reported a bis(borolide) complex [K(2.2.2)][[1-(piperidino)-2,3,4,5-tetraphenylborolyl]$_2$Dy] complex;[5a] and (*iii*) a bis(borolide) compound [K(18-crown-6)][$Dy(BC_4Ph_5)_2$] reported by Long et al.[5b] The latter two are Single-Ion Magnets (SIMs) with very high blocking temperatures comparable to the best all carbon-based dysprosium SIMs.[6] In addition of these, carbaboranes were also used as ligands to obtain Dy and Tb SMMs, namely $[(thf)_3(\mu\text{-}H)_3Li]_2[\{\eta^5\text{-}C_6H_4\text{-}(CH_2)_2C_2B_9H_9\}Dy\{\eta^2\text{:}\eta^5\text{-}C_6H_4\text{-}(CH_2)_2C_2B_9H_9\}_2Li]$[7] and $[Li_5(THF)_{10}][\eta^6\text{-}(\mu\text{-}1,2\text{-}(o\text{-}C_6H_4\text{-}(CH_2)_2)\text{-}1,2\text{-}C_2B_{10}H_{10})_2Ln]$ (Ln = Tb, Dy, Ho, Er).[8] Another promising boraheterocycle is diboratabenzene, which so far has not been used as a ligand in lanthanide chemistry. Due to the formal substitution of two CH units in benzene by two BH^- units, diboratabenzene is a dianionic aromatic ring, suitable for the construction of sandwich complexes.[5n,9] Unsubstituted diboratabenzenes are highly reactive and only a few compounds are known featuring this ligand.[9–10] Starting from this highly reactive species, by annulation of one or two benzo groups to the diboratabenzene unit, the more stable 1,4-benzodiborinine or 9,10-diboratataanthracene (DBA) can be obtained, respectively.[3a,11,12b,13] However, the coordination chemistry of diboratataanthracene is considerably underdeveloped and limited to s- and late d-block elements. The first DBA complexes were reported by Siebert et al. in 1991 and were initially only limited to iron carbonyl compounds (Figure 1B).[11] In 1995, the same group synthesised the first metal DBA sandwich complexes [(Cp)Co(DMDBA)] (DMDBA = 9,10-dimethyl-9,10-diboratataanthracene), [(toluene)Fe(DMDBA)] and [(Cod)Ni-(DMDBA)][12b] (Cod = cyclooctadiene) (Figure 1C). One year later the two triple-decker compounds [(Cp)Co-(DMDBA)Co(Cp)] and [(Cp)Fe(DMDBA)Fe(Cp)] were obtained, in which the DMDBA ligand builds the middle deck (Figure 1D). All these compounds were synthesised starting from the neutral 12-π-electron 9,10-diboraanthracene compound. The reduction of 9,10-diboraanthracene with potassium led to the monoanionic $[DMDBA]^-$ and the dianionic species $[DMDBA]^{2-}$. The former was reacted with $NiBr_2$ to obtain the first homoleptic DMDBA sandwich complex $[(DMDBA)_2Ni]$.[13] The 14-π-electron diborataanthracene is highly reductive and was previously used by Wagner et al. in small-molecule activation without the need for coordinating metal.[14] Two decades after the preparation of the first DBA complexes, we report here the synthesis of the first diborataanthracene rare-earth complexes, showcasing diverse structural motifs and SMM properties.

Results and Discussion

To introduce the DBA scaffold into the coordination sphere of a rare-earth ion, the previously established half-sandwich complexes $[Ln^{III}(\eta^8\text{-}Cot^{TIPS})(BH_4)(thf)_x]$[15] (Ln = Y, Sm, Dy, Er; **1**-Ln; Cot^{TIPS} = 1,4-(^{i}Pr$_3$Si)$_2$C$_8$H$_6$, TIPS = triisopropylsilyl) (for the synthesis of the Y and Dy compounds see page S5 of the Supporting Information) were selected as precursors. Since the bulky TIPS groups should provide sufficient steric shielding, as well as solubility, in common organic solvents, the Cot^{TIPS} system was considered a suitable co-ligand. Salt elimination reactions between equimolar amounts of dipotassium 9,10-diethyl-9,10-diboratataanthracene $[K_2(DEDBA)]$ and **1**-Ln in THF yielded the heteroleptic sandwich complexes $[K(\eta^8\text{-}Cot^{TIPS})Ln^{III}(\eta^6\text{-}DEDBA)]$ (Ln = Y, Dy, Er; **2**-Ln) (Scheme 1, left). By reacting two equivalents of $[Ln^{III}$-

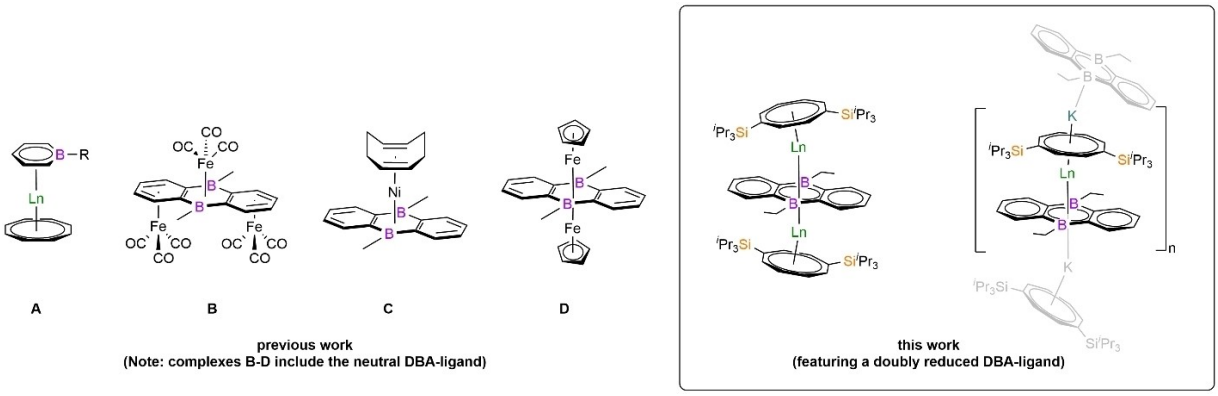

Figure 1. Molecular structures of $[Er^{III}(\eta^6\text{-}C_5H_5BMe)(\eta^8\text{-}Cot)]$ **A**,[5c] $[\{Fe(CO)_3\}_3(DMDBA)]$ **B**,[11] [Ni(COD)(DMDBA)] **C**,[12] $[\{Fe(Cp)\}_2(DMDBA)]$ **D**,[13] (DMDBA = 9,10-dimethyl-9,10-diboratataanthracene).

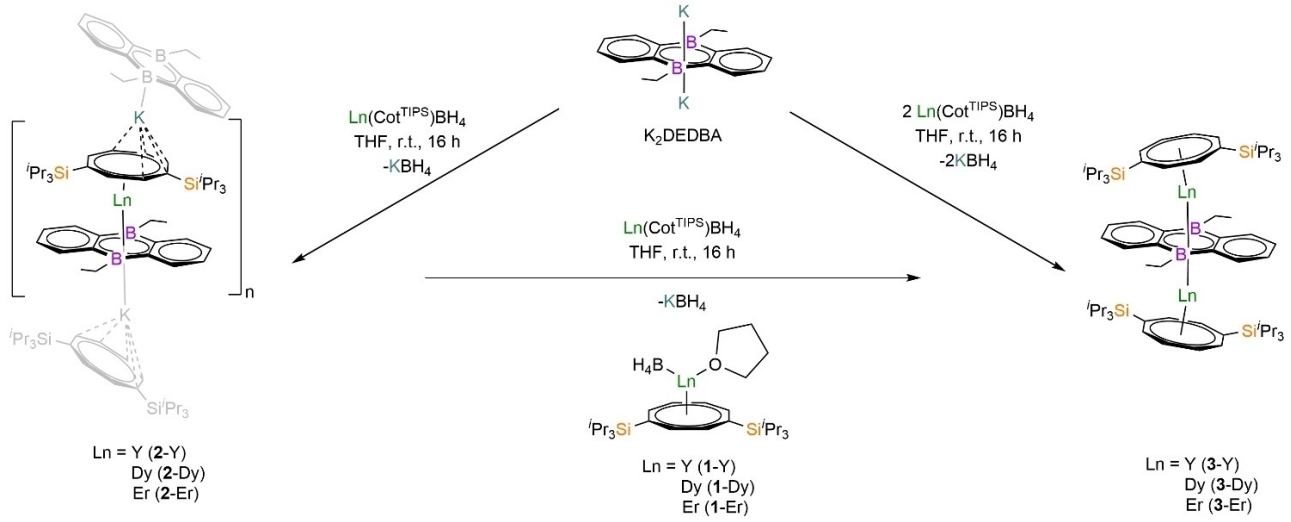

Scheme 1. Synthesis of compounds **2**-Ln and **3**-Ln. Attempts to synthesize the congeners of the larger lanthanides (La and Ce) to investigate the influence of the ionic radius on the bonding parameters were only successful in the case of **3**-Sm which is given in the ESI.

(η^8-Cot^{TIPS})(BH$_4$)(thf)$_x$] with one equivalent of [K$_2$-(DEDBA)], the heteroleptic triple-decker complexes **3**-Ln [(η^8-Cot^{TIPS})Ln^{III}(μ-η^6:η^6-DEDBA)Ln^{III}(η^8-Cot^{TIPS})] (Ln = Y, Dy, Er) were obtained (Scheme 1, right, for **3**-Sm see Supporting Information). After removal of the solvent *in vacuo*, the crude products were extracted with toluene and crystallised by slow evaporation of toluene (**2**-Ln) or from hot toluene (**3**-Ln) yielding the pure compounds as yellow to red crystalline materials (crystalline yields: **2**-Y: 47 %, **2**-Dy: 48 %, **2**-Er: 44 %, **3**-Y: 46 %, **3**-Dy: 39 %, **3**-Er: 42 %). Compounds **2**-Ln and **3**-Ln are, to the best of our knowledge the first rare-earth metal complexes comprising a diborataanthracene ligand. After crystallisation from toluene, the isostructural heteroleptic rare-earth complexes **2**-Ln (Ln = Y, Dy, Er) were obtained as Lewis-base free one-dimensional coordination polymers (Figure 2). The asymmetric unit consists of a [K(DEDBA)Ln^{III}(Cot^{TIPS})] moiety. Interestingly, the [(DEDBA)Ln^{III}(Cot^{TIPS})]$^-$ fragment coordinates an apical potassium ion in a μ-η^5:η^6 bridged coordination mode, which is additionally coordinated to the DEDBA ligand of the next repeating unit, thus forming the infinite 1D zigzag chain (Figure 2B). Similar behaviour has previously been reported by our group for the Lewis-base-free coordination polymer [KLn^{III}(Cot^{TIPS})]$_n$,[16] as well as in the lithium bridged polymer [Li(dme)Tb(Cot'')$_2$]$_n$[17] (Cot'' = 1,4-bis(trimethylsilyl)cyclooctatetraendiide). Binding to the η^6-DEDBA ligand occurs with K-Ct$_{DEDBA}$ (Ct = centroid of the corresponding ring) distances of 2.7233(11) Å (**2**-Y), 2.7423(7) Å (**2**-Dy) and 2.722(2) Å (**2**-Er), while the η^5-coordinated Cot^{TIPS} ligand shows K-Ct$_{Cot}$ distances of 2.647(1) Å (**2**-Y), 2.6617(7) Å (**2**-Dy) and 2.682(2) Å (**2**-Er). The formation of the zigzag structure mainly results from the slipped-off coordination mode of the Cot^{TIPS} ligand to the potassium ion with Ct$_{Cot}$-K-Ct$_{DEDBA}$ angles of 146.8° (**2**-Y, **2**-Dy) and 147.2° (**2**-Er). In contrast, the Cot^{TIPS}-Ln-DBA fragments are more coplanarly coordinated with Ct$_{Cot}$-Ln-Ct$_{DEDBA}$ angles of 160.7° (**2**-Y), 159.8° (**2**-Dy) and 162.0° (**2**-Er). As expected, the rare-earth ions are η^8-coordinated by the Cot^{TIPS} ligand and η^6-coordinated by the DEDBA ligand. The Ln-Ct$_{Cot}$ distances are found to be 1.7463(4) Å (**2**-Er), 1.7738(5) Å (**2**-Y) and 1.7906(3) Å (**2**-Dy), while for the Ln-Ct$_{DEDBA}$ distances the values of 2.2140(4) Å (**2**-Er), 2.2362(5) Å (**2**-Y) and 2.2619(3) Å (**2**-Dy) are obtained in accordance with the decreasing ionic radii of the rare-earth metals (Dy^{III} > Y^{III} > Er^{III}, Table 1). The C–C and C–B bond lengths in the central C$_4$B$_2$ moiety of the diborataan-

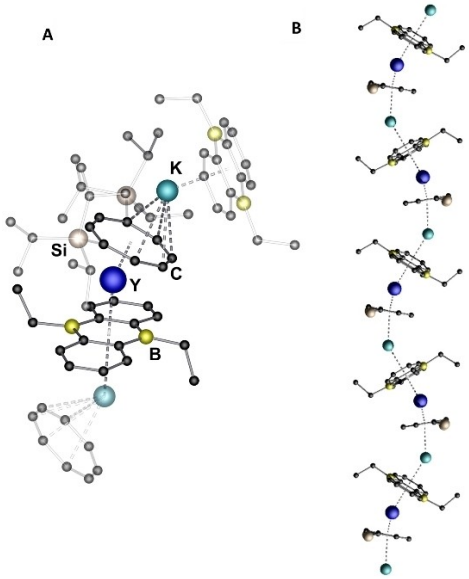

Figure 2. **A**: Molecular structure of [K(η^8-Cot^{TIPS})Y^{III}(η^6-DEDBA)] **2**-Y in the solid state. **B**: Section of the polymeric structure of **2**-Y. Hydrogen atoms are omitted, and silyl-groups as well as neighbouring monomeric units are transparent for clarity. Selected bond lengths and bond angles can be found in the ESI. Colour code: B: yellow, C: black, Si: beige, K: turquoise, Y: dark blue.[21]

Table 1: Selected bond lengths and -angles of compounds **2**-Ln.

Compound	**2**-Y	**2**-Dy	**2**-Er
Ln-Ct_{Cot} [Å]	1.7738(5)	1.7906(3)	1.7463(4)
Ln-Ct_{DEDBA} [Å]	2.2362(5)	2.2619(3)	2.2140(4)
K-Ct_{Cot} [Å]	2.647(1)	2.6617(7)	2.682(2)
K-Ct_{DEDBA} [Å]	2.7233(11)	2.6617(7)	2.822(2)
Ct_{Cot}-K-Ct_{DEDBA} [°]	146.75(4)	146.81(3)	147.24(6)
Ct_{DEDBA}-Ln-Ct_{Cot} [°]	160.74(3)	159.75(2)	161.98(2)

thracene ligand range between 1.450(8)-1.460(13) Å and 1.509(13)-1.545(7) Å, respectively, indicating retention of the aromatic nature of the ligand upon coordination to the rare-earth ion. Since no meaningful NMR spectra could be obtained for compounds **2**-Dy and **2**-Er due to their paramagnetic nature, compound **2**-Y was investigated by NMR spectroscopy as a diamagnetic model compound. In the ^{11}B NMR spectrum of compound **2**-Y, one resonance at $\delta = 30.6$ ppm was detected. Compared to the potassium salt of the ligand, this resonance is shifted approximately 3.6 ppm towards higher frequencies.[14a] The ^{89}Y NMR spectrum shows one resonance at $\delta = -72.6$ ppm which is considerably shifted towards lower frequencies compared to the starting material $[Y^{III}(\eta^8\text{-}Cot^{TIPS})(BH_4)(thf)]$ ($\delta = 44.9$ ppm). The shifts in the ^{11}B NMR and ^{89}Y NMR spectra can both be attributed to the increased electron density at the rare-earth ion upon coordination with the DEDBA ligand. All resonances in the ^{1}H, ^{13}C and ^{29}Si spectra can be assigned to the DEDBA and Cot^{TIPS} ligands.

The addition of one equivalent of $[Ln^{III}(\eta^8\text{-}Cot^{TIPS})(BH_4)(thf)_x]$ to the corresponding compound **2**-Ln or by the reaction of two equivalents of $[Ln^{III}(\eta^8\text{-}Cot^{TIPS})(BH_4)(thf)_x]$ (Ln = Y, Dy, Er) with $[K_2DEDBA]$, the triple-decker complexes **3**-Ln were obtained (Scheme 1, bottom and right). Contrary to the previously discussed coordination polymers **2**-Ln, the heteroleptic triple-deckers $[(\eta^8\text{-}Cot^{TIPS})Ln^{III}(\mu\text{-}\eta^6\text{:}\eta^6\text{-}DEDBA)Ln^{III}(\eta^8\text{-}Cot^{TIPS})]$ **3**-Ln (Ln = Y, Dy, Er) crystallise as monomers in which the DEDBA ligand constitutes the middle-deck (for **3**-Sm see Supporting Information). The asymmetric unit contains two $[(Cot^{TIPS})Ln^{III}]^+$ units bridged by an $\mu\text{-}\eta^6\text{:}\eta^6$-coordinated $[DEDBA]^{2-}$ middle deck. Despite the synthesis of numerous lanthanide complexes incorporating heterocyclic ligands, the successful construction of a triple-decker complex encompassing a six-membered ring, or a heterocycle has remained elusive. For the rare-earths only one further example of such a triple-decker is known. This is the Sc compound $[\{(\eta^5\text{-}P_3C_2{}^tBu_2)Sc\}_2(\mu\text{-}\eta^6\text{:}\eta^6\text{-}P_3C_3{}^tBu_3)]$ which was prepared by co-condensation of scandium vapour with an excess of ^{t}BuCP.[18]

Compounds **3** are therefore, to the best of our knowledge, the first trivalent lanthanide triple-decker compounds containing a six-membered ring and also the first lanthanide triple-decker featuring a heterocycle in their coordination sphere. The triple-deckers **3** are centrosymmetric, with the central Ct_{DEDBA} forming the centre of inversion. The crystallographic asymmetric units of **3**-Y, **3**-Dy and **3**-Er comprise two independent fragments with slightly different structural parameters. A similar crystallisation behaviour has been found in $[(Cot'')Ho\{\mu\text{-}\eta^8\text{:}\eta^8\text{-}C_8H_6(SiMe_3)_2\text{-}1,5\}Ho(Cot'')]$, one of the first linear triple-decker lanthanide sandwich complexes.[19] By comparing the Ln-Ct_{Cot} and Ln-Ct_{DEDBA} distances of compound **3**-Ln with those found for compound **2**-Ln, significant deviations are found (Table 2 and Table 1). Upon coordination of a second $[(Cot^{TIPS})Ln^{III}]^+$ moiety to the DEDBA ligand, the Ln-Ct_{Cot} distances are decreased on average by 0.047 Å (**3**-Y), 0.069 Å (**3**-Dy) and 0.049 Å (**3**-Er) for the two slightly different occurring molecules. The distances observed are in a similar range compared to other rare-earth sandwiches and multidecker complexes featuring the Cot moiety.[16a,19–20] Simultaneously, the Ln-Ct_{DEDBA} distances are increased by 0.059 Å (**3**-Y), 0.022 Å (**3**-Dy) and 0.050 Å (**3**-Er) in comparison to **2**-Ln. This is most likely caused by equal distribution of the electron density from the DEDBA ligand over both rare-earth ions in **3-**Ln, whereas in the presence of a potassium ion in **2-**Ln, more electron density is transferred to one single rare-earth ion.

As a result, the Cot^{TIPS} ligand moves closer to the rare-earth ions in the triple-decker complexes **3-**Ln and would expectedly increase the anisotropic properties of the erbium ions in **3**-Er, due to the Cot^{TIPS} ligand exerting a more equatorial ligand field.

The Cot^{TIPS}-Ln-DEDBA fragments are slightly bent with Ct_{Cot}-Ln-Ct_{DEDBA} angles of 162.3° (**3**-Y), 161.0° (**3**-Dy) and 162.9° (**3**-Er), while the Ln-Ct_{DEDBA}-Ln angle is perfectly linear with 180.0° for all cases of **3**-Ln. Compared to the compounds **2-**Ln, only a slight widening of the angles was observed. Presumably due to the large steric hindrance of the TIPS moieties, both Cot^{TIPS} ligands are tilted to opposite sides and thus adopt a kind of anti-periplanar conformation (Figure 3). NMR spectroscopic studies of compound **3**-Y reveal the chemical inequivalence of the two outer Cot^{TIPS} ligands. Thus, for each ligand, a separate set of signals was detected in the ^{1}H, ^{13}C and ^{29}Si NMR spectrum, respectively. One resonance was seen in the ^{11}B NMR at $\delta = -13.2$ ppm indicating the symmetric nature of the coordinated DEDBA ligand. The ^{89}Y NMR spectrum shows only one resonance at $\delta = -10.5$ ppm which is shifted towards higher frequencies compared to **1**-Y ($\delta = -72.6$ ppm) as expected by replacement of $[K]^+$ with $[(Cot^{TIPS})Y]^+$.

Table 2: Average bond lengths of Compounds **3-Ln**. Compounds **3-Ln** crystallise with two molecules in the asymmetric unit, each.

Compound	**3**-Y		**3**-Dy		**3**-Er	
	Molecule 1	Molecule 2	Molecule 1	Molecule 2	Molecule 1	Molecule 2
Ln-Ct_{Cot} [Å]	1.7241(3)	1.7303(3)	1.7183(5)	1.7254(5)	1.6941(3)	1.7012(3)
Ln-Ct_{DEDBA} [Å]	2.2905(3)	2.3005(3)	2.2787(6)	2.2891(5)	2.2577(3)	2.2709(3)

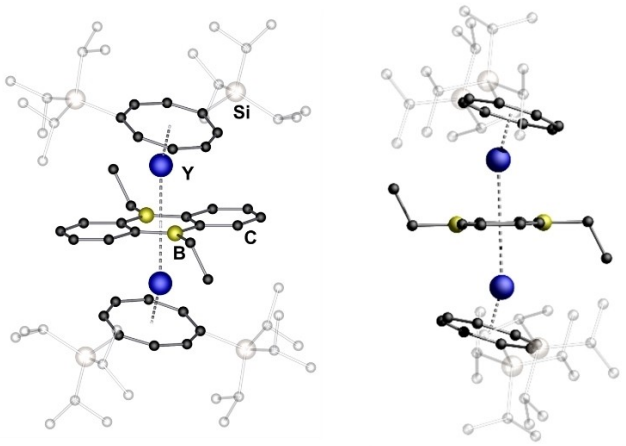

Figure 3. Molecular structures of [(η⁸-Cot^{TIPS})Y(μ-η⁶:η⁶-DEDBA)Y(η⁸-Cot^{TIPS})] **3**-Y in the solid state. Hydrogen atoms are omitted, and silyl-groups are transparent for clarity. Selected bond lengths and bond angles can be found in the ESI. Colour code: B: yellow, C: black, Si: beige, Y: dark blue.

Static magnetic studies: magnetic investigations of polycrystalline forms of the complexes **2**-Dy, **2**-Er, **3**-Dy and **3**-Er were carried out in an applied DC field of 1k Oe. As shown in Figure 4 and Figure S48, the room temperature $\chi_M T$ values for **2**-Dy (14.1 cm^3 K mol^{-1}), **2**-Er (11.3 cm^3 K mol^{-1}), **3**-Dy (27.8 cm^3 K mol^{-1}), and **3**-Er (22.4 cm^3 K mol^{-1}) are in the range of the expected values for the isolated Dy^{III} and Er^{III} ions - 14.2 cm^3 K mol^{-1} and 28.2 cm^3 K mol^{-1} for one and two Dy^{III}, respectively, with $g_J = 4/3$ and $J = 15/2$ and 11.5 cm^3 K mol^{-1} and 22.9 cm^3 K mol^{-1} for one and two Er^{III}, respectively, with $g_J = 6/5$ and $J = 15/2$). For complexes **2**-Dy and **2**-Er, cooling from 300 K resulted in a gradual decrease of the $\chi_M T$ down to 50 K and 150 K, respectively. Subsequently, an abrupt (**2**-Dy) and steady (**2**-Er) drop in the values were observed. At 2 K, the $\chi_M T$ reaches values of 4.0 cm^3 K mol^{-1} (**2**-Dy) and 6.7 cm^3 K mol^{-1} (**2**-Er). The decrease in the $\chi_M T$ values at low temperatures is generally attributed to the depopulation of the excited crystal field (m_J) levels, the presence of magnetic anisotropy, as well as inter- and/or intramolecular magnetic interactions. Considering the Ln···Ln distances observed in **2**-Dy and **2**-Er, intramolecular magnetic interactions contributing to the $\chi_M T(T)$ drop are ruled out. The measured and calculated $\chi_M T$ values agree very well for **2**-Dy while the decrease of experimental curve of **2**-Er is not found in the calculations (see Figure S48). This indicates a possible

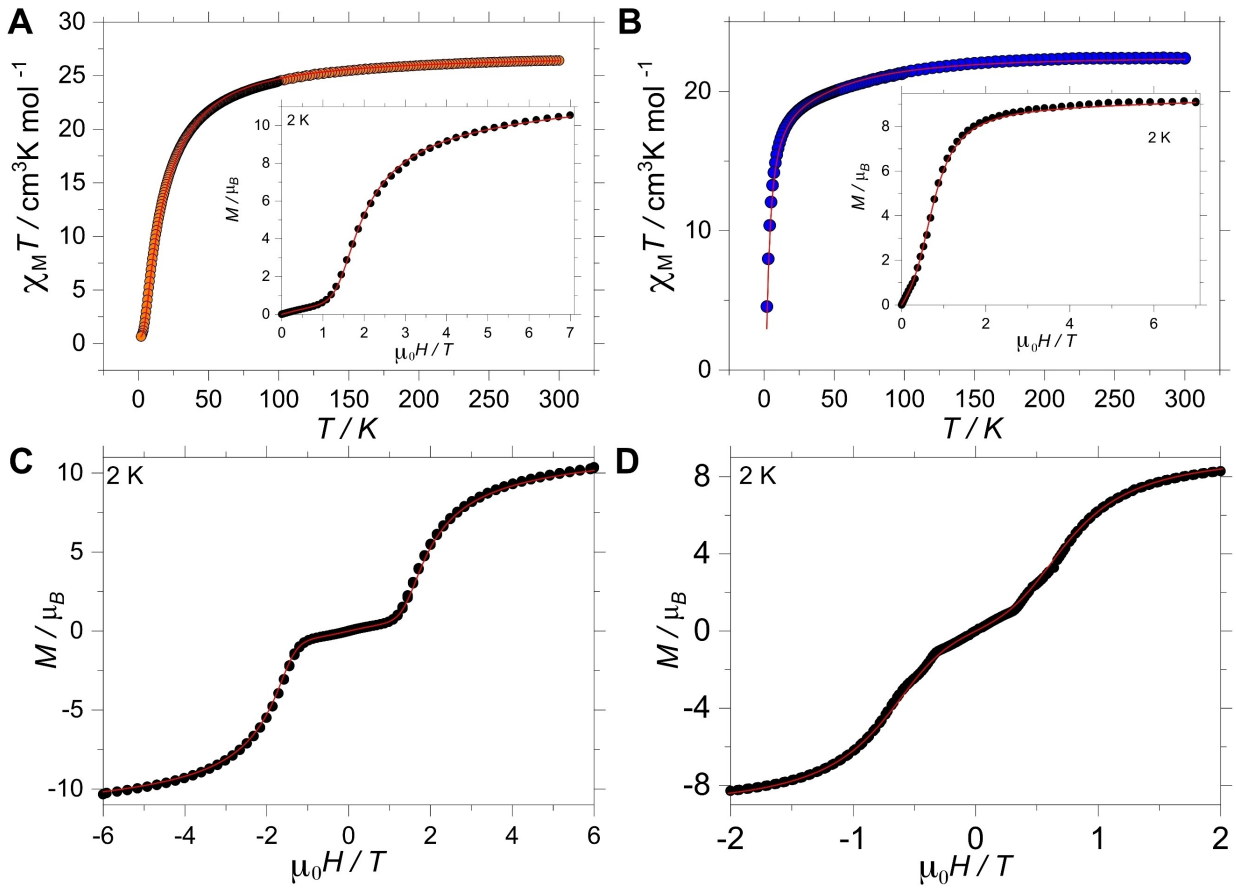

Figure 4. (**A**) Magnetic susceptibility ($\chi_M T(T)$ and $\chi_M(T)$) data for complexes **2-Er**. The solid traces are fit employing the parameters described in the text; (**B**) $\chi''_M(\nu)$ and (**C**) Cole-Cole and data with fits (solid lines) employing a generalised Debye model; (**D**) $\tau(T)$ data obtained from the Debye analysis and the fits to different relaxation processes using eq. 1 as described in the text.

intermolecular interaction. For complexes **3**-Dy and **3**-Er, a similar gradual decrease in the $\chi_M T$ values followed by a steady decrease at low temperatures was observed. At 2 K, $\chi_M T$ values of 0.65 cm^3 K mol^{-1} and 4.55 cm^3 K mol^{-1}, were obtained for **3**-Dy and **3**-Er, respectively. Given the dimeric nature of these complexes, such small values could be attributed to the intramolecular antiferromagnetic and/or dipolar interactions between the lanthanide centres, as well as to the depopulation of excited crystal field states.

The field dependence of magnetisation ($M(H)$) of the complexes was studied in a field range from 0 to 7 T and from 2 to 5 K (see insets in Figure 4 and S48). For **2**-Dy and **2**-Er, the $M(H)$ rapidly increase up to about 2 T and then gradually saturate. At 7 T, $M(H)$ values of 5.34 μ_B and 4.44 μ_B were obtained for **2**-Dy and **2**-Er, respectively. These values are close to the expected value for single Dy^{III} and Er^{III} centres, indicating population polarisation in the $m_J = \pm 15/2$ ground crystal-field states of the complexes. In contrast, for **3**-Dy and **3**-Er a different $M(H)$ profile was observed at 2 K. For **3**-Dy, $M(H)$ is nearly flat up to ca. 1.1 T, indicative of a diamagnetic state. Above 1.1 T, $M(H)$ increases rapidly reaching a maximum value of 10.5 μ_B at 7 T. For **3**-Er the $M(H)$ increases almost linearly up to around 0.4 T, where it increases faster up to ca. 2 T. After this field, $M(H)$ gradually reaches saturation (9.2 μ_B). In both cases, the low field behaviour is indicative of an antiferromagnetic coupling between the spin centres (*vide infra*). The antiferromagnetic coupling operating between the lanthanides is confirmed by the S-shaped hysteresis loops (Figure 4B, C). For **3**-Dy, a clear crossing is observed at ± 1.57 T, while for **3**-Er the crossing occurs at ± 0.58 T. The crossing between the antiferromagnetic ground state and the ferromagnetic excited state allows the direct estimation of the exchange coupling J_{ex} between the two Ln(III) ions through $H_{ex} = J_{ex} m_J / g_J \mu_\beta$, where $m_J = 15/2$, $g_{JDy} = 4/3$, $g_{JEr} = 6/5$, μ_β is the Bohr magneton. J_{ex} is found to be -0.065 cm^{-1} for **3**-Dy and -0.022 cm^{-1} for **3**-Er.

Dynamic magnetic studies: the relaxation dynamics of all complexes were studied employing alternating current (AC) magnetic susceptibility studies without and with applied DC fields. Frequency- and temperature-dependent AC studies under zero-applied fields show **2**-Dy, **2**-Er and **3**-Er are zero-field SMMs (Figure 5 and S49). For **2**-Dy, a maximum in the out-of-phase ($\chi''_M(\nu)$) is observed at 2 K centred at ca. 700 Hz and shifts slowly upon increasing temperatures up to 5.25 K, where the maximum shifts outside the experimental conditions. In contrast, the maximum observed for **2**-Er is centred at ca. 10 Hz and spans the temperature range of 2 to 9 K, indicating slower relaxation characteristics than the one observed for **2**-Dy. Upon warming, the maximum remains practically constant up to ca. 5 K, then it shifts swiftly up to 9 K. The faint shift in the $\chi''_M(\nu)$ maximum highlights that

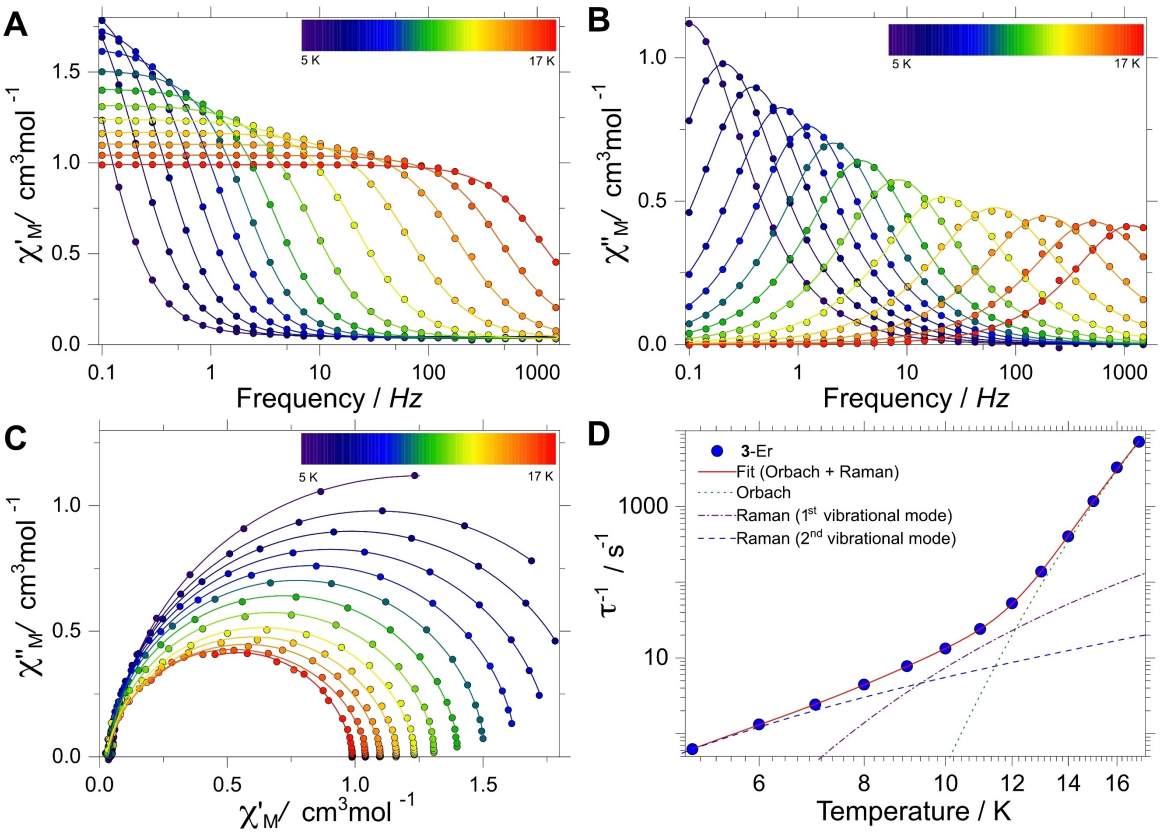

Figure 5. (**A**) in-phase ($\chi'_M(\nu)$), (**B**) out-of-phase magnetic susceptibility ($\chi''_M(\nu)$) and (**C**) Cole-Cole plots and fits (solid lines) to a generalised Debye model for **3**-Er. (**D**) Temperature dependence of the relaxation times ($\tau(T)$) obtained from the generalised Debye analysis for **3**-Er. The lines in $\tau(T)$ are the fits to different relaxation processes using eq. 1 as described in the text.

Quantum Tunnelling of the Magnetisation (QTM) is operative within the complexes. Note that although Dy^{III} and Er^{III} required different ligand fields due to their prolate and oblate nature, respectively, both systems are found to be SMMs. This can be a consequence of the axial/equatorial competence of the ligand field exerted in the systems.[5c,20c,22]

No SMM signature without and with applied DC fields was observed for **3**-Dy. Interestingly, for **3**-Er a clear SMM behaviour is observed, with a clear maximum in the $\chi''_M(\nu)$ between 5 and 17 K. In contrast to **2**-Dy and **2**-Er, where the $\chi''_M(\nu)$ maximum features QTM relaxation, for **3**-Er, we find that the maximum shifts swiftly upon increasing temperatures, indicating that QTM is not visible at the temperature of the study. The frequency-dependent data for **2**-Dy, **2**-Er, and **3**-Er can be fitted to a generalised Debye model allowing the extraction of the temperature-dependent relaxation times ($\tau(T)$). The relaxation characteristics for all complexes were fitted to:

$$\tau^{-1} = \tau_0^{-1}\exp^{-U_{\text{eff}}/kT} + \sum_{i=1}^{2} C \frac{\exp(\hbar\omega_i/k_B T)}{{}_i\left(\exp\left(\frac{\hbar\omega_i}{k_B T}\right)-1\right)^2} + \tau_{\text{QTM}}^{-1} \qquad (1)$$

where the first term is the Orbach process, the second the Raman and the third the QTM relaxation processes. In the Raman term ω_i represents vibrational mode contributing to this mechanism.

For **2**-Dy solely the Raman, with a single vibrational mode, and QTM processes are sufficient to account for $\tau(T)$ with the best-fit yielding, $C_1 = 10(3)\times10^3\ s^{-1}$, $\omega_1 = 5.2(5)\ cm^{-1}$, and $\tau_{QTM} = 2.43(3)\times10^{-4}$ s (Figure S49B). For **2**-Er, a good fit is obtained accounting for the Orbach process, one vibrational Raman mode and the QTM processes, leading to the following parameters: $\tau_0 = 9(5)\times10^{-9}$ s, $U_{\text{eff}} = 60(3)\ cm^{-1}$, $C_1 = 4(2)\times10^2\ s^{-1}$, $\omega_1 = 7(1)\ cm^{-1}$, and $\tau_{QTM} = 1.17(2)\times10^{-2}$ s (Figure S49D). For **3**-Er, the best fits requires the inclusion of the Orbach processes and two vibrational Raman modes affording $\tau_0 = 1.0(1)\times10^{-10}$ s, $U_{\text{eff}} = 167(2)\ cm^{-1}$, and $C_1 = 6(3)\times10^3\ s^{-1}$, $\omega_1 = 47(4)\ cm^{-1}$, $C_2 = 27(13)\ s^{-1}$ and $\omega_2 = 13(2)\ cm^{-1}$ (Figure 5D). The ω_i are found to be small, as expected for molecular systems.[23]

Comparing the U_{eff} found for **3**-Er with other Cot-containing Er^{III} systems, we can observe that it falls in the range of reported systems (see Table 3).[5c,24] It can also be seen that the U_{eff} for **3**-Er is smaller than the $[Er_2(Cot'')_3]$ complex, implying that η^6-DEDBA exerts a weaker equatorial ligand field than the Cot^{2-} counterpart.[20d] Another factor playing a role in the lower U_{eff} of **3**-Er compared to $[Er_2(Cot'')_3]$ is the less planar arrangement of the COT, compared to $[Er_2(Cot'')_3]$,[20d] which can decrease the gap between the doublets states of the system.[21]

Theoretical studies: to comprehend the static and dynamic magnetic characteristics of the complexes, ab-initio calculations were carried out for all complexes employing the experimental crystal structures with optimisation of the hydrogen atoms only. Complete Active Space Spin-Orbit Configuration Interaction (CASOCI)[27] calculations were carried out considering the 4f orbitals as active space. For details see section quantum chemical calculations in the Supporting Information. For **2**-Dy, a ground doublet with $g_x \approx g_y \approx 0$ and $g_z \approx 20$, characteristic of an $m_J = \pm15/2$ state was obtained, as confirmed by the wavefunction composition. The ground Kramers doublet is separated from the first excited doublet by ca. 80 cm^{-1}, with the second and third excited doublets being at 98 and 155 cm^{-1}, respectively. For **2**-Er, a similar behaviour is obtained, i.e., a highly axial ground doublet with $g_x \approx g_y \approx 0$ and $g_z \approx 18$ and a large $m_J = \pm15/2$ state composition. In **2**-Er, a smaller separation, 44 cm^{-1}, between the ground and first excited state is found, with the second and third excited states being at 75 and 88 cm^{-1}, respectively. For **3**-Dy, we find a slightly more mixed ground doublet with a 95 % $m_J = \pm15/2$ and 5 % $\pm11/2$ composition, while the first excited state resides at ca. 52 cm^{-1}. In contrast, **3**-Er possesses a highly pure $m_J = \pm15/2$ (99 %) ground doublet with the first excited state lying at ca. 100 cm^{-1}. As shown in Figure 6, the anisotropy axis for **2**-Er and **3**-Er is almost perpendicular (85 °) to the DBA ligand plane, while for **2**-Dy and **3**-Dy, the angles are much smaller, i.e., 56° and 38°, respectively (Figure S56). With the knowledge of the crystal field parameters obtained from the *ab*-initio calculations (Table S14), it is possible to simulate[28] the static magnetic behaviour for **2**-Dy and **2**-Er. The $\chi_M T(T)$ and $M(H)$ plots can be simulated employing a Hamiltonian of the following form:

$$\mathcal{H} = \mathcal{H}_{lf} + g_J\mu_0\mu_B\hat{\boldsymbol{J}}\boldsymbol{H}_z \qquad (2)$$

where $\mathcal{H}_{lf} = \sum_{k=2,\,4,\,6,\,-k\le q\le k} B_k^q O_k^q$ is the ligand field Hamiltonian expressed in the extended Stevens operators, O_k^q , B_k^q are the crystal field parameters obtained from CASOCI calculations, $\boldsymbol{H}_z$ is the magnetic field and μ_0 and μ_B are the vacuum permittivity and the Bohr magneton, respectively. The results are shown in Figure 4 (solid lines).

To account for the dimeric nature of **3**-Dy and **3**-Er and to evaluate the interaction operating between the lanthanide ions, the Lines model was employed to fit $\chi_M T(T)$ and $M(H)$. The Lines model[29] employs an isotropic exchange between the spin component of the angular momenta ($S = 5/2$ for Dy^{III} and $S = 3/2$ for Er^{III}) and the crystal field parameters obtained via the CASOCI calculations. The Hamiltonian has the form:

Table 3: Experimental energy barriers for Cot-Er-based systems.

	Compounds[#]	U_{eff} / cm^{-1}	Ref.
1	$[(C_5H_5BMe)Er(Cot)]$	300	[5c]
2	$[(C_5H_5BH)Er(Cot)]$	259	[5c]
3	$[(Cnt)Er(Cot)]$	251	[24a]
4	$[(Dsp)Er(Cot)]$	248	[24b]
5	$[Er_2(Cot'')_3]$	225	[20d]
6	$[(C_5H_5BNEt_2)Er(Cot)]$	174	[5c]
7	$[(\eta^8\text{-}Cot^{TIPS})Er(\mu\text{-}\eta^6{:}\eta^6\text{-}DEDBA)Er(\eta^8\text{-}Cot^{TIPS})]$	167	This work
8	$[Er(Cot)_2]^-$	147	[25]
9	$[(\eta^5\text{-}C_5Me_5))Er(Cot)]$	137/225	[26]
10	$[Er(Cot'')_2]^-$	134	[24c]

[#] $Cot = \eta^8\text{-}C_8H_8$, $Cnt = C_9H_9$, $Dsp^- = 3,4\text{-dimethyl-2,5-bis(trimethylsilyl)phospholy}$

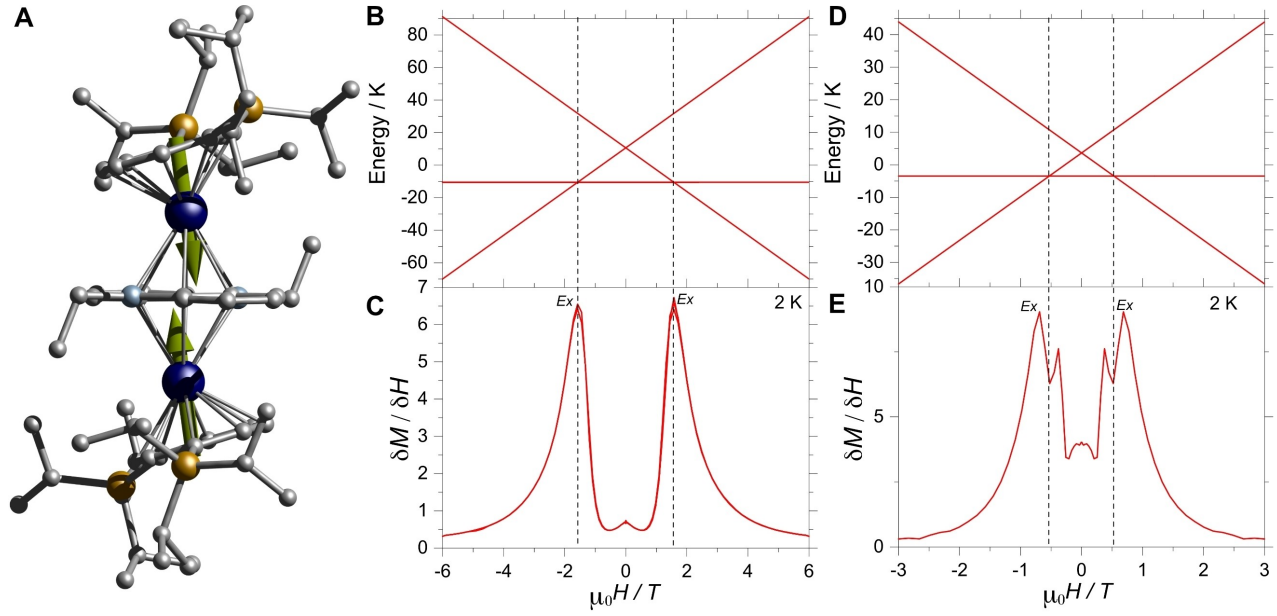

Figure 6. (**A**) Anisotropy axes obtained from CASOCI calculations for **3**-Er. Colour code: Ln, dark blue; C, grey; Si, orange; K, pink; B, pale blue. (**B-E**) Zeeman diagrams (top) and derivative of the hysteresis loops (bottom) for **3**-Dy (**B**, **C**) and **3**-Er (**D**, **E**) highlighting the crossing between the antiferromagnetic ground state and the ferromagnetic excited state for both complexes employing J_{ex}. A similar energy diagram is obtained employing the Lines model.

$$\mathcal{H} = \sum_{i=1}^{2}\left(\mathcal{H}_{lf}^{i} + g_J\mu_0\mu_B\widehat{J}_i\boldsymbol{H}_z\right) + -2J_{Lines}\widehat{S}_1\widehat{S}_2 \qquad (3)$$

where the sum runs over the one-centre Hamiltonians (eq. 2) of the two Ln^{III} centres and the second term is the interaction operating between the spin components of the lanthanide ions. $\widehat{J}_i$ and $\widehat{S}_i$ are the spin-orbit and spin-only states for the Ln^{III} ions, respectively. Simultaneous fitting of $\chi_M T(T)$ and $M(H)$, employing the crystal field parameters determined from CASOCI, results in $J_{Lines} = -0.497(4)$ cm^{-1} for **3**-Dy and $-0.358(1)$ cm^{-1} for **3**-Er (Figure 4 and insets). Note that the best fit for **3**-Dy requires the inclusion of 3 % monomeric impurity and $zJ = -0.03$ cm^{-1}.

The crossings between the antiferromagnetic ground state and the first excited state are better observed in the derivative of the $M(H)$ data (Figure 6 C, D). A direct comparison between J_{ex} and J_{Lines} is not trivial, however, the crossings between the antiferromagnetic ground state and the ferromagnetic excited state are reproduced by both models. Because of the strong anisotropy, the collinearity of the magnetic axes, and the $m_J = 15/2$ character of the lowest Kramers doublet, J_{ex} and J_{Lines} can be scaled to an Ising type coupling of two $\tilde{S} = 1/2$ pseudo spins for the lowest Kramers doublet with factors of 225 for J_{ex} and 25 and 9 for J_{Lines} for Dy^{III} and Er^{III}, respectively. The resulting values are in reasonable agreement with $J\left(\tilde{S} = 1/2\right) = -14.625$ cm^{-1} $(-12.425$ $cm^{-1})$ for **3**-Dy and $J\left(\tilde{S} = 1/2\right) = -4.950$ cm^{-1} $(-3.222$ $cm^{-1})$ for **3**-Er calculated from J_{ex} and J_{Lines} (numbers in brackets). Comparison between the experimentally determined J_{ex} and the dipolar exchange from a pure point dipolar approximation shows that the magnetic dipolar interaction, $J_{ij}^{dip}\left(\tilde{S} = 1/2\right)$, is considerably smaller than the antiferromagnetic coupling. For a Dy···Dy distance of 4.5783(8) Å the dipolar interactions are $J_{xx}^{dip} = +4.2\times10^{-4}$ cm^{-1} $(+9.5\times10^{-2}$ $cm^{-1})$, $J_{xz}^{dip} = J_{zx}^{dip} = +3.4\times10^{-4}$ cm^{-1} $(+7.6\times10^{-2}$ $cm^{-1})$, $J_{zz}^{dip} = +2.7\times10^{-4}$ cm^{-1} $(+6.1\times10^{-2}$ $cm^{-1})$, all other $J_{ij}^{dip} = 0$. For an Er···Er distance of 4.495(8) Å the dipolar interactions are $J_{xx}^{dip} = +1.5\times10^{-4}$ cm^{-1} $(+3.3\times10^{-2}$ $cm^{-1})$, $J_{xz}^{dip} = J_{zx}^{dip} = +9.8\times10^{-4}$ cm^{-1} $(+0.22$ $cm^{-1})$, $J_{zz}^{dip} = +6.5\times10^{-3}$ cm^{-1} $(+1.46$ $cm^{-1})$, all other being $J_{ij}^{dip} = 0$. Note that the J_{ij}^{dip} are projected on a $m_J = \pm 15/2$ state (numbers in brackets refer to $\left(\tilde{S} = 1/2\right)$, the coordinate system of the dipolar matrix is chosen with respect to the Ln–Ln connection axis, see Dipolar Matrix section in the Supporting Information for details).

At this point, and with the knowledge of the electronic characteristics of the complexes, it is also possible to rationalise the static and dynamic properties. The SMM character for **2**-Dy and **2**-Er arise from the anisotropic characteristics of the ground doublet states, which are separated by 44 and 80 cm^{-1} from the first excited state, respectively. Employing the square of the average matrix elements of magnetic moment between the electronic states as a proxy for the relaxation of the systems, it can be noticed that relaxation is highly viable via the first excited state and through QTM and Raman processes. This is supported by the $\tau(T)$ fits (Figures 5B and 5D). It is important to notice

that the $\chi''_M(\nu;T)$) for **2**-Er is shifted to lower frequencies and higher temperatures compared to **2**-Dy, highlighting more axial character in **2**-Er, which could be attributed to the ligand stabilising better prolate ion, than an oblate one.

In contrast, when placing a second ion nearby, two situations are attained. For **3**-Dy no SMM signatures were observed. This behaviour can be a direct consequence of the mixing of the not highly pure state, which is coupled through a relatively strong antiferromagnetic interaction, causing the system to relax faster than in **2**-Dy. In this case, the interaction instead of causing an exchange bias-type of behaviour, where tunnelling is drifted away from zero field, the interaction creates further relaxation pathways by mixing the ground state wave functions. Contrary to the behaviour of the Dy^{III} dimer, **3**-Er shows a clear SMM behaviour at zero field with no signature of active QTM. The SMM character can be rationalised by a highly pure ground state composition, which despite the interaction, remains highly axial in the dimer. Furthermore, the absence of QTM at zero field is a direct consequence of the exchange bias interaction between the Er^{III} ions, which causes the QTM crossing to shift towards higher fields. Comparing **2**-Er and **3**-Er, the experimentally observed barriers agree with the energies of the first excited Kramers doublet in **2**-Er and with the second excited Kramers doublet in **3**-Er, respectively. In **3**-Er, the relaxation pathway via the first excited Kramers doublet of the Er ions seem to be blocked, possibly by the high anisotropy of the second Kramers doublet with the main axes tilted by only 33° with respect to the ground state.

Conclusion

In summary, we introduced the highly reductive dianionic DEDBA ligand for the first time into the coordination sphere of a rare-earth element, leading to two types of sandwich complexes. First, the anionic sandwich complexes **2**-Ln are formed as Lewis-base free one-dimensional coordination polymers when crystallized from toluene. Notably, compounds **2-**Dy and **2**-Er exhibit SMM behaviour, with the erbium complex featuring an energy barrier of 93 K. Secondly, we synthesised the triple-decker complexes **3**-Ln which represent not only the first triple-decker complexes of the lanthanides including a six-membered ring but also the first trivalent lanthanide triple-decker featuring a heterocycle in the coordination sphere. For magnetic behaviour, two different cases are attained by the introduction of a second lanthanide ion. In the case of **3**-Dy, no SMM signatures were observed, this arises from state impurity mixing via relatively strong antiferromagnetic interaction, accelerating relaxation compared to **2**-Dy, and enhancing relaxation paths by mixing ground state wave functions. In contrast, **3**-Er shows clear SMM behaviour with an energy barrier of 235 K and open hysteresis. Notably, no signature of active QTM at zero field is observed, this is a direct consequence of the exchange bias interaction between the Er^{III} ions, which causes the QTM crossing to shift towards higher fields. Our approach also highlights the importance of interaction in SMMs, which can allow the enhancements of their magnetic properties via Ln···Ln interactions. Moreover, we highlight how the half-sandwich Er-Cot monomer can act as a scaffold for the construction of polymetallic systems, in which the ligand with the appropriate equatorial ligand field could be constructed and exploited. In addition, the flexibility of the Er-Cot scaffold plays a crucial role in the synthesis of otherwise inaccessible Cot-Er–L type complexes. The insertion of heterocycles additionally influences the geometry of the triple-decker complexes and the interactions between the lanthanide atoms. A full picture of the influence of heterocycles inserted into the magnetic properties of the Er-Cot scaffolds, would require more detailed analysis.

Supporting Information

Crystallographic data for the structures reported in this paper have been deposited with the Cambridge Crystallographic Data Centre as a supplementary publication no. 2309385–2309393.

Acknowledgements

The authors gratefully acknowledge support from the Deutsche Forschungsgemeinschaft (DFG, German Research Foundation) through the Collaborative Research Centre "4f for Future" (CRC 1573 project number 471424360, projects B1 and B3) and the Reinhart Koselleck-Projekt 440644676, RO 2008/19-1. CU thanks the Fonds der Chemischen Industrie for the generous fellowship (No. 108320). The Karlsruhe Nano Micro Facility (KNMF, www.kit.edu/knmf) is acknowledged for the provision of access to instruments at their laboratories. Open Access funding enabled and organized by Projekt DEAL.

Conflict of Interest

The authors declare no conflict of interest.

Data Availability Statement

The data that support the findings of this study are available in the supplementary material of this article.

Keywords: coordination chemistry · boron chemistry · heterocycle · lanthanides · triple-decker complexes

[1] T. J. Kealy, P. L. Pauson, *Nature* **1951**, *168*, 1039.
[2] a) F. T. Edelmann, in *Metallocenes*, **1998**, pp. 55; b) F. Jäkle, J. B. Sheridan, *Angew. Chem. Int. Ed.* **2008**, *47*, 7587; c) A. Zabala-Lekuona, J. M. Seco, E. Colacio, *Coord. Chem. Rev.* **2021**, *441*, 213984.

[3] a) W. Siebert, in *Adv. Organomet. Chem., Vol. 35* (Eds.: F. G. A. Stone, R. West), Academic Press, **1993**, pp. 187; b) G. E. Herberich, W. Boveleth, B. Hessner, M. Hostalek, D. P. J. Köffer, M. Negele, *J. Organomet. Chem.* **1987**, *319*, 311.

[4] a) G. E. Herberich, B. Buller, B. Hessner, W. Oschmann, *J. Organomet. Chem.* **1980**, *195*, 253; b) G. E. Herberich, G. Greiss, H. F. Heil, *Angew. Chem. Int. Ed.* **1970**, *9*, 805; c) A. J. Ashe III, P. Shu, *J. Am. Chem. Soc.* **1971**, *93*, 1804.

[5] a) J. C. Vanjak, B. O. Wilkins, V. Vieru, N. S. Bhuvanesh, J. H. Reibenspies, C. D. Martin, L. F. Chibotaru, M. Nippe, *J. Am. Chem. Soc.* **2022**, *144*, 17743; b) A. H. Vincent, Y. L. Whyatt, N. F. Chilton, J. R. Long, *J. Am. Chem. Soc.* **2023**, *145*, 1572; c) Y.-S. Meng, C.-H. Wang, Y.-Q. Zhang, X.-B. Leng, B.-W. Wang, Y.-F. Chen, S. Gao, *Inorg. Chem. Front.* **2016**, *3*, 828; d) P. Cui, Y. Chen, G. Wang, G. Li, W. Xia, *Organometallics* **2008**, *27*, 4013; e) P. Cui, Y. Chen, X. Zeng, J. Sun, G. Li, W. Xia, *Organometallics* **2007**, *26*, 6519; f) P. Cui, Y. Chen, G. Li, W. Xia, *Angew. Chem. Int. Ed.* **2008**, *47*, 9944; g) X. Wang, W. Peng, P. Cui, X. Leng, W. Xia, Y. Chen, *Organometallics* **2013**, *32*, 6166; h) B. Wang, X. Zheng, Gerhard E. Herberich, *Eur. J. Inorg. Chem.* **2002**, 31; i) X. Zheng, B. Wang, U. Englert, G. E. Herberich, *Inorg. Chem.* **2001**, *40*, 3117; j) X. Fang, X. Li, Z. Hou, J. Assoud, R. Zhao, *Organometallics* **2009**, *28*, 517; k) C. Wang, X. Leng, Y. Chen, *Organometallics* **2015**, *34*, 3216; l) Y. Yuan, X. Wang, Y. Li, L. Fan, X. Xu, Y. Chen, G. Li, W. Xia, *Organometallics* **2011**, *30*, 4330; m) M. A. Putzer, J. S. Rogers, G. C. Bazan, *J. Am. Chem. Soc.* **1999**, *121*, 8112; n) V. Paprocki, P. Hrobárik, K. L. M. Harriman, M. S. Luff, T. Kupfer, M. Kaupp, M. Murugesu, H. Braunschweig, *Angew. Chem. Int. Ed.* **2020**, *59*, 13109; o) G. E. Herberich, U. Englert, A. Fischer, J. Ni, A. Schmitz, *Organometallics* **1999**, *18*, 5496; p) D. Zhu, M. Wang, L. Guo, W. Shi, J. Li, C. Cui, *Organometallics* **2021**, *40*, 2394; q) C. Wang, L. Xiang, X. Leng, Y. Chen, *Organometallics* **2016**, *35*, 1995; r) X. Wang, X. Leng, Y. Chen, *Dalton Trans.* **2015**, *44*, 5771; s) P. Cui, Y. Chen, G. Li, W. Xia, *Organometallics* **2011**, *30*, 2012; t) C. Wang, L. Xiang, X. Leng, Y. Chen, *Dalton Trans.* **2017**, *46*, 1218; u) X. Fang, Y. Deng, Q. Xie, F. Moingeon, *Organometallics* **2008**, *27*, 2892; v) Y. Yuan, Y. Chen, G. Li, W. Xia, *Organometallics* **2010**, *29*, 3722.

[6] a) F.-S. Guo, B. M. Day, Y.-C. Chen, M.-L. Tong, A. Mansikkamäki, R. A. Layfield, *Science* **2018**, *362*, 1400; b) K. Randall McClain, C. A. Gould, K. Chakarawet, S. J. Teat, T. J. Groshens, J. R. Long, B. G. Harvey, *Chem. Sci.* **2018**, *9*, 8492; c) F.-S. Guo, B. M. Day, Y.-C. Chen, M.-L. Tong, A. Mansikkamäki, R. A. Layfield, *Angew. Chem. Int. Ed.* **2017**, *56*, 11445; d) C. A. P. Goodwin, F. Ortu, D. Reta, N. F. Chilton, D. P. Mills, *Nature* **2017**, *548*, 439.

[7] P.-B. Jin, Y.-Q. Zhai, K.-X. Yu, R. E. P. Winpenny, Y.-Z. Zheng, *Angew. Chem. Int. Ed.* **2020**, *59*, 9350.

[8] P.-B. Jin, K.-X. Yu, Q.-C. Luo, Y.-Y. Liu, Y.-Q. Zhai, Y.-Z. Zheng, *Angew. Chem. Int. Ed.* **2022**, *61*, e202203285.

[9] a) M. Dietz, M. Arrowsmith, L. Endres, V. Paprocki, B. Engels, H. Braunschweig, *J. Am. Chem. Soc.* **2023**, *145*, 22222; b) G. E. Herberich, B. Heßner, *Chem. Ber.* **1982**, *115*, 3115.

[10] M. Arrowsmith, J. Böhnke, H. Braunschweig, M. A. Celik, C. Claes, W. C. Ewing, I. Krummenacher, K. Lubitz, C. Schneider, *Angew. Chem. Int. Ed.* **2016**, *55*, 11271.

[11] H. Schulz, H. Pritzkow, W. Siebert, *Chem. Ber.* **1991**, *124*, 2203.

[12] a) P. Müller, S. Huck, H. Köppel, H. Pritzkow, W. Siebert, *Zeitschrift für Naturforschung B* **1995**, *50*, 1476; b) P. Müller, B. Gangnus, H. Pritzkow, H. Schulz, M. Stephan, W. Siebert, *J. Organomet. Chem.* **1995**, *487*, 235.

[13] P. Mu"ller, H. Pritzkow, W. Siebert, *J. Organomet. Chem.* **1996**, *524*, 41.

[14] a) E. von Grotthuss, S. E. Prey, M. Bolte, H.-W. Lerner, M. Wagner, *J. Am. Chem. Soc.* **2019**, *141*, 6082; b) A. Lorbach, M. Bolte, H.-W. Lerner, M. Wagner, *Organometallics* **2010**, *29*, 5762; c) E. von Grotthuss, M. Diefenbach, M. Bolte, H.-W. Lerner, M. C. Holthausen, M. Wagner, *Angew. Chem. Int. Ed.* **2016**, *55*, 14067; d) E. von Grotthuss, S. E. Prey, M. Bolte, H.-W. Lerner, M. Wagner, *Angew. Chem. Int. Ed.* **2018**, *57*, 16491; e) S. E. Prey, C. Herok, F. Fantuzzi, M. Bolte, H.-W. Lerner, B. Engels, M. Wagner, *Chem. Sci.* **2023**, *14*, 849.

[15] a) L. Münzfeld, X. Sun, S. Schlittenhardt, C. Schoo, A. Hauser, S. Gillhuber, F. Weigend, M. Ruben, P. W. Roesky, *Chem. Sci.* **2022**, *13*, 945; b) S. M. Cendrowski-Guillaume, G. Le Gland, M. Nierlich, M. Ephritikhine, *Organometallics* **2000**, *19*, 5654.

[16] a) L. Münzfeld, A. Hauser, P. Hädinger, F. Weigend, P. W. Roesky, *Angew. Chem. Int. Ed.* **2021**, *60*, 24493; b) A. Hauser, L. Münzfeld, C. Uhlmann, S. Lebedkin, S. Schlittenhardt, T.-T. Ruan, M. M. Kappes, M. Ruben, P. W. Roesky, *Chem. Sci.* **2024**.

[17] V. Lorenz, A. Edelmann, S. Blaurock, F. Freise, F. T. Edelmann, *Organometallics* **2007**, *26*, 6681.

[18] P. L. Arnold, F. G. N. Cloke, P. B. Hitchcock, J. F. Nixon, *J. Am. Chem. Soc.* **1996**, *118*, 7630.

[19] A. Edelmann, V. Lorenz, C. G. Hrib, L. Hilfert, S. Blaurock, F. T. Edelmann, *Organometallics* **2013**, *32*, 1435.

[20] a) V. Lorenz, S. Blaurock, C. G. Hrib, F. T. Edelmann, *Organometallics* **2010**, *29*, 4787; b) F. T. Edelmann, *New J. Chem.* **2011**, *35*, 517; c) J. J. Le Roy, M. Jeletic, S. I. Gorelsky, I. Korobkov, L. Ungur, L. F. Chibotaru, M. Murugesu, *J. Am. Chem. Soc.* **2013**, *135*, 3502; d) J. J. Le Roy, L. Ungur, I. Korobkov, L. F. Chibotaru, M. Murugesu, *J. Am. Chem. Soc.* **2014**, *136*, 8003.

[21] Deposition Numbers 2309385 (for 1-Y), 2309386 (for 1-Dy), 2309387 (for 2-Y), 2309388 (for 1-Dy), 2309389 (for 1-Er), 2309390 (for 3-Y), 2309391 (for 3-Sm), 2309392 (3-Dy), 2309393 (for 3-Er) contains the supplementary crystallographic data for this paper. These data are provided free of charge by the joint Cambridge Crystallographic Data Centre and Fachinformationszentrum Karlsruhe Access Structures service.

[22] a) M. D. Korzyński, M. Bernhardt, V. Romankov, J. Dreiser, G. Matmon, F. Pointillart, B. Le Guennic, O. Cador, C. Copéret, *Chem. Sci.* **2022**, *13*, 10574; b) M. Jeletic, P.-H. Lin, J. J. Le Roy, I. Korobkov, S. I. Gorelsky, M. Murugesu, *J. Am. Chem. Soc.* **2011**, *133*, 19286; c) M.-M. Ding, T. Shang, R. Hu, Y.-Q. Zhang, *Dalton Trans.* **2022**, *51*, 3295; d) K. L. M. Harriman, M. Murugesu, *Acc. Chem. Res.* **2016**, *49*, 1158.

[23] a) F. S. Santana, M. Perfetti, M. Briganti, F. Sacco, G. Poneti, E. Ravera, J. F. Soares, R. Sessoli, *Chem. Sci.* **2022**, *13*, 5860; b) M. Briganti, F. Santanni, L. Tesi, F. Totti, R. Sessoli, A. Lunghi, *J. Am. Chem. Soc.* **2021**, *143*, 13633; c) J. Wang, J. J. Zakrzewski, M. Zychowicz, Y. Xin, H. Tokoro, S. Chorazy, S.-i. Ohkoshi, *Angew. Chem. Int. Ed.* **2023**, *62*, e202306372.

[24] a) L. Münzfeld, C. Schoo, S. Bestgen, E. Moreno-Pineda, R. Köppe, M. Ruben, P. W. Roesky, *Nat. Commun.* **2019**, *10*, 3135; b) S.-M. Chen, J. Xiong, Y.-Q. Zhang, Q. Yuan, B.-W. Wang, S. Gao, *Chem. Sci.* **2018**, *9*, 7540; c) J. J. Le Roy, I. Korobkov, M. Murugesu, *Chem. Commun.* **2014**, *50*, 1602.

[25] K. R. Meihaus, J. R. Long, *J. Am. Chem. Soc.* **2013**, *135*, 17952.

[26] S.-D. Jiang, B.-W. Wang, H.-L. Sun, Z.-M. Wang, S. Gao, *J. Am. Chem. Soc.* **2011**, *133*, 4730.

[27] T. Bodenstein, A. Heimermann, K. Fink, C. van Wüllen, *ChemPhysChem* **2022**, *23*, e202100648.

[28] N. F. Chilton, R. P. Anderson, L. D. Turner, A. Soncini, K. S. Murray, *J. Comput. Chem.* **2013**, *34*, 1164.

[29] M. Lines, *J. Chem. Phys.* **1971**, *55*, 2977.

Manuscript received: January 19, 2024
Accepted manuscript online: February 23, 2024
Version of record online: March 22, 2024